PCCP

ROYAL SOCIETY OF CHEMISTRY

PAPER

Published on 14 May 2026
Licensed under CC-BY 4.0

Check for updates

Cite this: *Phys. Chem. Chem. Phys.*, 2026, **28**, 13111

# Improved SABRE hyperpolarisation using pulse sequences to reduce effective coupling

Vitaly P. Kozinenko, †[a] Bogdan A. Rodin, †[a] James Eills, [b] Ilai Schwartz, [a] Stephan Knecht *[a] and Laurynas Dagys *[c]

Received 9th March 2026,
Accepted 29th April 2026

DOI: 10.1039/d6cp00879h

rsc.li/pccp

Hyperpolarisation using signal amplification by reversible exchange (SABRE) is a convenient method for high repeatability studies. The core of this technique is polarisation transfer to the target substrate during an ongoing chemical exchange process. Typically, polarisation transfer is achieved as fast as possible. In this study, we employ NMR sequences that on the contrary slow down the polarisation transfer and yet demonstrate improved performance. Simulations confirm that such methods can lead to high polarisation yield in SABRE systems where hydride protons exhibit stronger magnetic inequivalence and substrates exchange with a lower rate.

## 1 Introduction

Hyperpolarisation techniques offer a promising solution to the inherently low sensitivity of nuclear magnetic resonance (NMR) spectroscopy. These methods enhance sensitivity by increasing nuclear spin-polarisation through various interactions with an external source of spin-order.[1–25] A class of methods known as parahydrogen-induced polarisation (PHIP) derives signal enhancement from a chemical reaction with a specific spin isomer of hydrogen called parahydrogen.[1–23] The nuclei of parahydrogen, which are entangled in a nuclear singlet state, relay this state onto a target molecule by hydrogenation reaction. Then, the singlet-order in the sample is converted into the magnetisation of the target spins using a variety of possible NMR sequences or magnetic field cycling. PHIP stands out as a cost-effective hyperpolarisation methodology with growing interest in the fields of medical imaging and metabolomics.[2,4–7,12]

A promising PHIP variant offering high repeatability and low cost is called signal amplification by reversible exchange (SABRE).[2–23] It utilizes a catalyst, typically iridium-based, that supports reversible formation of a parahydrogen–substrate complex instead of irreversible hydrogenation. The magnetisation of the target nuclei is converted from the singlet state of the attached parahydrogen using various polarisation transfer schemes. Reversible chemical exchange then releases the substrate to the solution, which gradually builds up polarisation in the free substrate pool. The substrate is not consumed during the SABRE process, meaning that polarisation can be restored with a constant supply of parahydrogen gas. This makes the SABRE method a cost-effective hyperpolarisation method, finding applications in drug detection and *ex situ* metabolomics, and rapidly advancing towards *ex vivo* studies.[4–7,9,26]

SABRE stems from a fine-tuned interplay between chemical exchange and spin dynamics. Finding suitable SABRE conditions often requires extensive and careful optimisation of both polarisation transfer and exchange rates as their matching determines the overall efficiency. For example, too fast chemical exchange makes the substrate–parahydrogen complex short-lived and does not allow polarisation transfer to effectively build up magnetisation in the substrate pool. Therefore, one known strategy to increase SABRE efficiency is to slow down chemical exchange by lowering the temperature.[8,26] This is especially effective for hyperpolarisation of weak SABRE ligands like $^{13}$C-pyruvate, where polarisation transfer is limited by the weak (sub-hertz) spin–spin coupling between the hydride protons and the $^{13}$C site.[9–12] Other substrates, particularly $^{15}$N-labelled heterocycle systems, form complexes with strong spin–spin coupling to the hydrides, leading to much faster spin dynamics and polarisation build-up. However, once the heteronuclear spin–spin coupling becomes larger than the proton homonuclear coupling in the hydride, it induces a strong magnetic inequivalence for the $^{1}$H sites in the complex. This considerably alters the dynamics of singlet-order to magnetisation conversion, rendering the SABRE methodology sensitive to the optimisation of the applied NMR sequences.[13–15,27]

In this work, we analyse two different NMR sequences: double-radio-frequency spin lock-induced crossing (DRF-SLIC) and PulsePol. Polarisation transfer with simultaneous excitation on the proton and heteronuclear channels, analogous to

[a] *NVision Imaging Technologies GmbH, Wolfgang-Paul Straße 2, 89081 Ulm, Germany. E-mail: stephan@nvision-imaging.com*
[b] *Forschungszentrum Jülich, Wilhelm-Johnen-Straße, 52428 Jülich, Germany*
[c] *Institute of Chemical Physics, Vilnius University, Saulėtekio av. 3, Vilnius LT10257, Lithuania. E-mail: laurynas.dagys@ff.vu.lt*
† These authors contributed equally to this work.

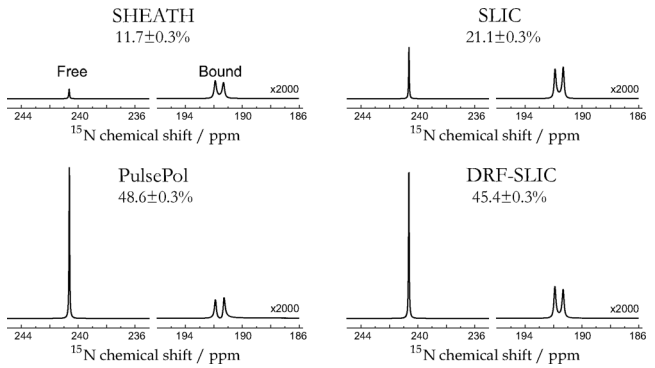


Fig. 1 The $^{15}$N spectra of hyperpolarised $^{15}$N-acetonitrile recorded after four different SABRE protocols. Polarisation levels of the free substrate species are provided above each spectrum. Deviation is estimated by repeating experiments four times. See Section 2.3 for more experimental details.

DRF-SLIC, was previously employed for hydrogenative PHIP in symmetrical molecules[28,29] and SABRE at high magnetic fields,[16,17,30] although its potential for scaling the coupling was not harnessed or examined in detail. PulsePol was developed as a robust pulse sequence for the transfer of electron polarisation to nuclei,[24,25] but later proved to be efficient for PHIP applications.[31,32] In this study, we successfully utilise the capacity of these sequences to effectively reduce heteronuclear spin–spin coupling in the SABRE complex. We compared these methods to the more established SABRE-SHEATH and SABRE-SLIC protocols and applied them to three different target substrates – $^{15}$N-acetonitrile, $^{15}$N-pyridine and metronidazole.[11,19–23,33] Although DRF-SLIC and PulsePol differ in their design, they both achieved a similar striking performance in hyperpolarisation of $^{15}$N-acetonitrile (Fig. 1). We hypothesise that this is linked to increased magnetic equivalence of the hydrides and reduced polarisation transfer rate, approaching the rate of chemical exchange.

This is confirmed by numerical simulations and by decreased observed performance in $^{15}$N-pyridine and metronidazole systems, which exhibit an increasingly faster chemical exchange rate. We therefore believe that methods like DRF-SLIC or PulsePol can outperform other methods in many SABRE systems exhibiting similar dynamic range. The additional degree of freedom in the DRF-SLIC and PulsePol methods may potentially lead to improvements in other SABRE applications, further promoting the use of hyperpolarisation in routine NMR practice.

# 2 Methods

## 2.1 Materials

Three SABRE solutions were studied. Each solution was prepared by first dissolving 3 mM of [IrCl(IMes)(COD)] and the specified substrates in methanol-$d_4$, followed by activation of the catalyst with hydrogen gas for a few minutes in an NMR pressure tube. For the $^{15}$N-acetonitrile, the solution contained 10 mM of $^{15}$N-acetonitrile as a substrate and 20 mM of pyridine as a co-substrate. The $^{15}$N-pyridine and metronidazole solutions contained 30 mM of the respective substrate.

The $^{15}$N-acetonitrile, $^{15}$N-pyridine, metronidazole, and methanol-$d_4$ were purchased from Sigma Aldrich, while [IrCl(IMes)(COD)] was synthesised from [Ir(COD)Cl$_2$] and 1,3-bis(2,4,6-trimethylphenyl)imidazol-2-ylidene (IMes) using a protocol described in the literature.[34,35]

Parahydrogen was produced by an Advanced Research Systems (ARS) parahydrogen generator packed with an iron monohydrate catalyst, running at 22 K temperature and producing gas which was stored in aluminium bottles at a pressure of 30 bar. Parahydrogen was supplied to the SABRE solutions at 10 bar of pressure using a pressure regulator and electronically controlled valves.

## 2.2 Equipment

All experiments were performed using an automated system comprising a 9.4 T Bruker superconducting magnet, a Bruker Avance NEO NMR console, a TwinLeaf MS-1 μ-metal shield equipped with home-built coils, and a sample shuttling system integrated with a solenoid valve array managing the gas flow. Hydrogen gas was supplied to 5 mm pressure NMR tubes using 1/16″ Teflon and 0.2 mm fused silica capillaries. The entire system was controlled *via* a custom Python script running on a separate computer. The static bias field during SABRE protocols was produced by a solenoid coil powered by a Rhode&Schwartz HMP2030 power supply. The oscillating transverse field was generated *via* the analogue output of a National Instruments PXIe-6363 card and amplified by a home-built audio amplifier. The waveforms for the low-field NMR sequences were calculated using the custom Python script and digitised at a 400 kHz sampling rate.

High-field $^{15}$N NMR spectra of 200 ppm width were collected using 64k points by exciting the SABRE-polarised samples with a single 17 μs 90° pulse. The $^{15}$N enhancement factors were estimated by collecting thermally polarised $^{15}$N spectra of the SABRE samples with $^{1}$H decoupling at room temperature using 300 transients with a repetition delay of 200 s. Spectra were baseline corrected.

## 2.3 SABRE experiments

The experiments in this study were performed following the procedure outlined in Fig. 2 using the automated experimental setup. Activated SABRE solutions were transported to a low-field area where fresh parahydrogen was supplied *via* bubbling. The bubbling period lasted 20 s, during which SABRE protocols, shown in Fig. 3, were executed. After the samples were polarised, bubbling was ceased, and the samples were shuttled to the high field NMR magnet for data acquisition.

Experiments involving spin-lock induced crossing (SLIC) utilised a bias field of 98 μT and a transverse field resonant with $^{15}$N spins. The nutation frequency of the SLIC pulse was optimised within the range of 0–30 Hz for each substrate. See the supplementary information (SI) for more information. Following the application of the SLIC pulse, the carrier frequency of the transverse field was linearly decreased by 50 Hz

 This journal is © the Owner Societies 2026

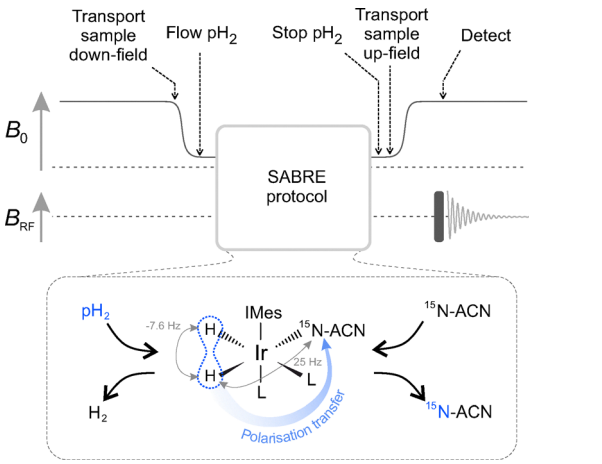


Fig. 2 General scheme of the SABRE protocol. First, the sample is moved from the NMR magnet to a low magnetic field. Then, parahydrogen bubbling is initiated, followed by the polarisation transfer pulse sequence. Once the sequence is finished, bubbling is stopped and the sample is moved back to the magnet for recording of the NMR spectra. The inset shows the active SABRE complex between parahydrogen and $^{15}$N-acetonitrile. Relevant $J$-couplings are indicated in grey.[36] Letters "L" indicate other possible competing ligands, such as pyridine.

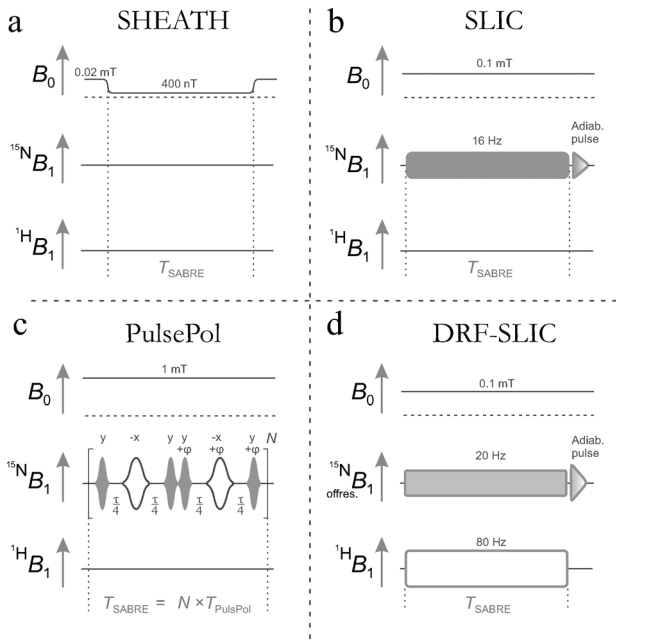


Fig. 3 Low-field polarisation transfer sequences applied as depicted in Fig. 2 for hyperpolarisation of $^{15}$N compounds at low magnetic field. (a) SHEATH involves ramping the magnetic field down to approximately 400 nT for the duration of the bubbling. (b) Spin-lock induced crossing (SLIC) is performed at a fixed magnetic field of 98 μT by applying a transverse field $B_1$ on $^{15}$N resonance with an amplitude of ~16 Hz. A final adiabatic pulse is applied to flip $^{15}$N magnetization along the bias field axis before sample transportation. (c) The PulsePol method is performed at a bias field of 1 mT. Filled and unfilled shapes represent 90° and 180° shaped pulses, respectively, with Gaussian shape truncated at 10%. The number of repetitions ($N$) is set to match bubbling time $T_{SABRE}$. Duration $\tau$ and phase $\varphi$ were adjusted for optimal polarisation transfer. See more details in the text. (d) The double-radio-frequency SLIC (DRF-SLIC) protocol uses an on-resonance transverse field for $^1$H and off-resonant field for $^{15}$N nuclei. The resonance mismatch is adjusted for optimal polarization transfer. A final adiabatic pulse is applied to flip $^{15}$N magnetisation along the bias field axis before sample transportation.

over 1 second, while its amplitude was simultaneously decreased linearly to zero. This procedure ensured the adiabatic rotation of the created magnetisation, aligning it with the bias longitudinal field before sample shuttling.

The SHEATH protocol involved switching the magnetic field from 20 μT magnetic field to ultra-low magnetic field for the duration of the bubbling. The SHEATH field was optimised within the range of 0–2000 nT. After the bubbling with parahydrogen was finished, the magnetic field was switched back to 20 μT before the samples were shuttled back to the high field magnet.[37]

The PulsePol NMR sequence was tested at a bias field of 1 mT with a Gaussian pulse peak amplitude of 600 Hz. The shape ensured minimal Bloch–Siegert shift due to big pulse amplitudes and avoided the indirect excitation of $^1$H spins due to short pulse durations. The phase $\varphi$ and duration $\tau$ were experimentally optimised, using simulated values as an initial starting point. The number of PulsePol cycles was adjusted to match the 20 s duration of the bubbling process.

Final experiments utilising the double-RF SLIC (DRF-SLIC) method were performed at 98 μT bias field using two excitation channels, one resonant with $^1$H spins and the second slightly off-resonant with $^{15}$N spins. The transverse field amplitude for $^1$H was fixed at 80 Hz while for $^{15}$N the amplitude was fixed at 16–30 Hz with the resonance detuning of 60–100 Hz.

Tables with optimal values of key experimental parameters together with optimisation routines and an extensive simulation section are provided in the SI.

## 3 Adjusting the effective coupling

Optimising the SABRE efficiency requires a precise balance between coherent spin dynamics and dissociation of the SABRE-active complex (Fig. 2). Generally, higher dissociation rates also suit higher optimal polarisation transfer rates, but the precise correlation is non-trivial. Cases exist where the highest efficiency is expected once population exchange ($A^*$) is comparable with the dissociation constant ($k_d$), *i.e.*, $A^* \approx k_d$.[38] These relationships constitute the first tuning constraints on pulse sequence design in SABRE. Within the framework of level anti-crossing (LAC) theory, the population exchange rate is determined by the perturbation $V$ ($A^* = 2V$), which breaks the degeneracy of two interacting states.[39]

The second constraint, particularly relevant for nitrogen-containing heterocycles such as $^{15}$N-pyridine, stems from the spin-coupling regime. In SABRE complexes involving these molecules, the heteronuclear coupling $J_{NH}$ between the hydrides and the substrate $^{15}$N site often exceeds the homonuclear hydride coupling $J_{HH}$ leading to strong magnetic inequivalence in the spin system.[27,40] Consequently, the standard LAC condition overlaps with the other and leads to non-selective redistribution of populations to multiple spin states, interfering with the desired polarisation transfer. Therefore, reduced heteronuclear coupling

leads to narrow LAC conditions, restoring the isolated and efficient polarisation transfer.

Let us first consider the case of a 3 spin-1/2 system under the influence of a transverse oscillating field, slightly off-resonant for the $^{15}$N nuclei. Note that the method with an on-resonant field corresponds to a more known SLIC sequence.[33] In the rotating tilted frame, the secular and perturbing Hamiltonians can be written as:[16]

$$\begin{aligned}\hat{H} &= \hat{H}_0 + \hat{V}\\ \hat{H}_0 &= -\nu_0^{\mathrm{H}}\left(\hat{I}_{\mathrm{H},z}+\hat{I}_{\mathrm{H}',z}\right)-\nu_{\mathrm{eff}}^{\mathrm{N}}\hat{I}_{\mathrm{N},z}+J_{\mathrm{HH}}\hat{I}_{\mathrm{H}}\hat{I}_{\mathrm{H}'}\\ &\quad+J_{\mathrm{NH}}\frac{\cos\theta}{2}\left(\hat{I}_{\mathrm{H},z}\hat{I}_{\mathrm{N},z}+\hat{I}_{\mathrm{H}',z}\hat{I}_{\mathrm{N},z}\right)\\ \hat{V} &= J_{\mathrm{NH}}\frac{\cos\theta}{2}\left(\hat{I}_{\mathrm{H},z}\hat{I}_{\mathrm{N},z}-\hat{I}_{\mathrm{H}',z}\hat{I}_{\mathrm{N},z}\right)\\ &\quad-J_{\mathrm{NH}}\sin\theta\hat{I}_{\mathrm{H},z}\hat{I}_{\mathrm{N},x}\end{aligned} \tag{1}$$

where $\nu_{\mathrm{eff}}^{\mathrm{N}}=\sqrt{(\nu_{\mathrm{nut}}^{\mathrm{N}})^2+(\Omega^{\mathrm{N}})^2}$ is the effective frequency of the $^{15}$N nucleus rotating around the field tilted with respect to the static field by the angle defined by $\tan\theta=\frac{\nu_{\mathrm{nut}}^{\mathrm{N}}}{\Omega^{\mathrm{N}}}$. Here, $I$ denotes the spin-operator, $\nu_0$ is the Larmor frequency of the respective nucleus, $\Omega$ is the resonance offset, and $\nu_{\mathrm{nut}}^{\mathrm{N}}$ is the nutation frequency of the $^{15}$N nucleus. $J_{\mathrm{HH}}$ is the homonuclear coupling between the hydrides, $J_{\mathrm{HN}}$ is the heteronuclear coupling between one of the hydride protons and the $^{15}$N site and $J_{\mathrm{H'N}}$ is assumed to be zero for simplicity.

The eigenbasis of the secular Hamiltonian $\hat{H}_0$ can be found by taking the tensor product of proton singlet–triplet basis and $^{15}$N Zeeman basis, forming the so-called **STZ** basis, expressed as $\{|S\rangle,\ |T_0\rangle,\ |T_+\rangle,\ |T_-\rangle\}_{\mathrm{H}}\otimes\{|\alpha'\rangle,\ |\beta'\rangle\}_{\mathrm{N}}$, with $|S\rangle=\frac{1}{\sqrt{2}}(|\alpha\beta\rangle-|\beta\alpha\rangle)$, $|T_0\rangle=\frac{1}{\sqrt{2}}(|\alpha\beta\rangle+|\beta\alpha\rangle)$, $|T_+\rangle=|\alpha\alpha\rangle$, $|T_-\rangle=|\beta\beta\rangle$ and $\{|\alpha'\rangle,\ |\beta'\rangle\}_{\mathrm{N}}$ defined along the $z$-axis in the tilted frame. For the purposes of analysing polarisation transfer during the SABRE experiment, one can isolate the states of interest – $\{|S\alpha'\rangle,\ |S\beta'\rangle,\ |T_0\alpha'\rangle,\ |T_0\beta'\rangle\}$ and express the total Hamiltonian in the matrix form at the LAC condition ($\nu_{\mathrm{eff}}^{\mathrm{N}}=-J_{\mathrm{HH}}$):

$$\hat{H}=\begin{array}{c|cccc} & |S\alpha'\rangle & |S\beta'\rangle & |T_0\alpha'\rangle & |T_0\beta'\rangle\\ \hline \langle S\alpha'| & -\frac{5}{4}J_{\mathrm{HH}} & 0 & \frac{1}{4}J_{\mathrm{NH}}\cos\theta & -\frac{1}{4}J_{\mathrm{NH}}\sin\theta\\ \langle S\beta'| & -- & -\frac{1}{4}J_{\mathrm{NH}} & -\frac{1}{4}J_{\mathrm{NH}}\sin\theta & -\frac{1}{4}J_{\mathrm{NH}}\cos\theta\\ \langle T_0\alpha'| & -- & -- & -\frac{1}{4}J_{\mathrm{NH}} & 0\\ \langle T_0\beta'| & -- & -- & -- & \frac{3}{4}J_{\mathrm{HH}}\end{array} \tag{2}$$

At this condition, the otherwise degenerate states $|S\beta'\rangle$ and $|T_0\alpha'\rangle$ are perturbed and undergo population exchange. Assuming fully populated proton singlet states, this exchange alone is sufficient to achieve a fully polarised heteronucleus. The effective transition rate is given by the off-diagonal element $2V=2\langle S\beta'|\hat{H}_0|T_0\alpha'\rangle=\frac{-1}{2}J_{\mathrm{NH}}\sin\theta$. Note that for the conventional SLIC method, the detuning parameter is $\Omega^{\mathrm{N}}=0$ and tilt angle $\theta$ equals 90°, ensuring maximum rate of $\frac{1}{2}J_{\mathrm{NH}}$. Reduction of the effective angle can be used as the SABRE optimisation parameter for suitable matching to chemical exchange. However, in a three spin system with $|J_{\mathrm{NH}}|>|J_{\mathrm{HH}}|$, the perturbation connecting the $|S\alpha'\rangle$ and $|T_0\beta'\rangle$ states may be relatively large compared to their energy difference ($\Delta E=2J_{\mathrm{HH}}$). This can cause additional population exchange reducing the polarisation efficiency, which is consistent with our numerical SABRE simulation of the studied systems (see Fig. 4).

To solve this problem, we utilise double resonance DRF-SLIC, where an additional on-resonance transverse field is applied at the $^1$H channel. With additional on-resonance irradiation for protons, the quantisation axis is flipped. It results in:

$$\begin{aligned}\hat{H} &= \hat{H}_0 + \hat{V}\\ \hat{H}_0 &= -\nu_{\mathrm{nut}}^{\mathrm{H}}\left(\hat{I}_{\mathrm{H},z}+\hat{I}_{\mathrm{H}',z}\right)-\nu_{\mathrm{eff}}^{\mathrm{N}}\hat{I}_{\mathrm{N},z}+J_{\mathrm{HH}}\hat{I}_{\mathrm{H}}\hat{I}_{\mathrm{H}'}\\ &\quad+J_{\mathrm{NH}}\frac{\cos\theta}{2}\left(\hat{I}_{\mathrm{H},x}\hat{I}_{\mathrm{N},z}+\hat{I}_{\mathrm{H}',x}\hat{I}_{\mathrm{N},z}\right)\\ \hat{V} &= J_{\mathrm{NH}}\frac{\cos\theta}{2}\left(\hat{I}_{\mathrm{H},x}\hat{I}_{\mathrm{N},z}-\hat{I}_{\mathrm{H}',x}\hat{I}_{\mathrm{N},z}\right)\\ &\quad+J_{\mathrm{NH}}\sin\theta\hat{I}_{\mathrm{H},x}\hat{I}_{\mathrm{N},x}\end{aligned} \tag{3}$$

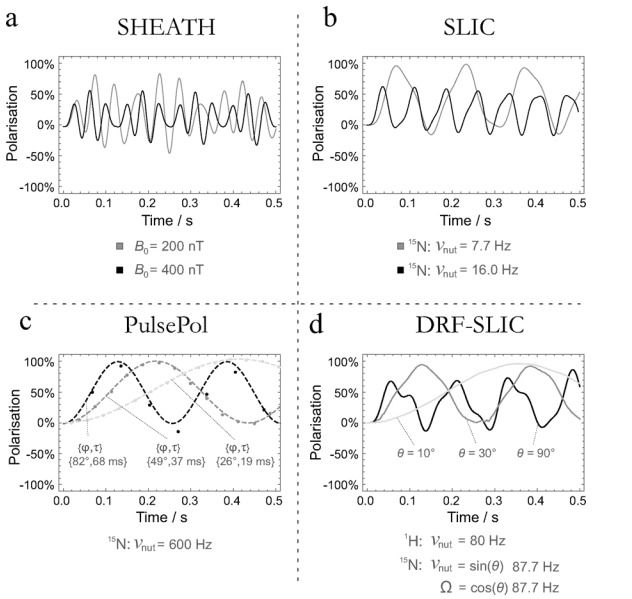


Fig. 4 Numerical simulation of different singlet-to-magnetisation transfer methods in the active $^{15}$N-acetonitrile SABRE complex (depicted in Fig. 2). (a) Simulations of SHEATH transfer at 200 nT and 400 nT magnetic fields are given in grey and black, respectively. (b) Polarisation transfer using the $^{15}$N on-resonance field depicted in grey and black for amplitudes 7.7 Hz and 16 Hz. (c) Numerical simulation of $^{15}$N magnetisation for each PulsePol cycle at different phase $\varphi$ and duration $\tau$ settings with the pulse amplitude set to 600 Hz. The sinusoidal curve is provided as a guide. (d) Simulation of polarisation transfer trajectories during the DRF-SLIC method is calculated according to the mathematical relations given below. Simulations are shown for three different effective angles $\theta$.


This journal is © the Owner Societies 2026

The resonance matching for DRF-SLIC is governed by the modified LAC condition: $\nu_{\mathrm{eff}}^{\mathrm{N}} = \nu_{\mathrm{nut}}^{\mathrm{H}} \pm J_{\mathrm{HH}}$. Here, the hydride spins are quantised along the $x$-axis of the rotating frame. We denote the resulting triplet states as $|T'\rangle$, while the singlet state $|S\rangle$ remains invariant under this rotation. The transition leading to heteronuclear polarisation transfer is $|S\beta'\rangle \rightarrow |T'_{-}\alpha'\rangle$ if the state $|S\alpha'\rangle$ is unperturbed. The partial matrix representation of the Hamiltonian at the LAC condition is given by:

$$\hat{H} = \begin{array}{c|cccc} & |S\alpha'\rangle & |S\beta'\rangle & |T'_{-}\alpha'\rangle & |T'_{-}\beta'\rangle \\ \hline \langle S\alpha'| & -\frac{1}{4}(5J_{\mathrm{HH}}+2\nu_{\mathrm{nut}}^{\mathrm{H}}) & 0 & -\frac{1}{4\sqrt{2}}J_{\mathrm{NH}}\cos\theta & \frac{1}{4\sqrt{2}}J_{\mathrm{NH}}\sin\theta \\ \langle S\beta'| & -- & -\frac{1}{4}(J_{\mathrm{NH}}-2\nu_{\mathrm{nut}}^{\mathrm{H}}) & \frac{1}{4\sqrt{2}}J_{\mathrm{NH}}\sin\theta & \frac{1}{4\sqrt{2}}J_{\mathrm{NH}}\cos\theta \\ \langle T'_0\alpha'| & -- & -- & -\frac{1}{4}(J_{\mathrm{NH}}-2\nu_{\mathrm{nut}}^{\mathrm{H}}) & 0 \\ \langle T'_0\beta'| & -- & -- & -- & -\frac{3}{4}(-J_{\mathrm{NH}}-2\nu_{\mathrm{nut}}^{\mathrm{H}}) \end{array} \quad (4)$$

where the rate of transition is $2V = \frac{2}{4\sqrt{2}}J_{\mathrm{NH}}\sin\theta$. Here, the key parameter is $\nu_{\mathrm{nut}}^{\mathrm{H}}$ as it allows shifting of the energy of the $|S\alpha'\rangle$ state and isolates it from all the other states. Numerical simulations support these considerations, demonstrating that DRF-SLIC achieves consistently higher polarisation compared to single-frequency SLIC in the slow and intermediate exchange regimes. In the fast-exchange limit ($k_{\mathrm{d}} > 100\ \mathrm{s}^{-1}$), both methods exhibit comparable efficiency.

**PulsePol** represents an alternative approach to singlet-to-magnetisation conversion. It relies on applying a pulse train to construct an effective interaction-frame Hamiltonian, so the evolution of one of its harmonics matches the evolution frequency of the coupled states. Detailed analysis of this sequence can be found elsewhere.[24]

In the context of the present study, the primary advantage of PulsePol is that, depending on the selected resonance condition, the sequence can effectively rescale the heteronuclear scalar coupling. This provides a precise mechanism for matching the polarisation transfer rate to the catalyst dissociation rate ($k_{\mathrm{d}}$), analogous to the control achieved *via* DRF-SLIC, but with potentially greater robustness to experimental offsets.

## 4 Results and discussion

The $^{15}$N polarisation levels achieved after experimental optimisation of each SABRE protocol for the three target molecules are presented in Fig. 6. We observe that the results with each target molecule vary considerably depending on the applied SABRE method. The most striking difference was observed on $^{15}$N-acetonitrile where DRF-SLIC and PulsePol led to 45% and 49%, respectively, compared to the more established SLIC and SHEATH methods (21% and 12%, respectively). This improvement is also qualitatively predicted by the numerical simulation (Fig. 5), although simulation suggests that DRF-SLIC should always outperform. As the PulsePol sequence offers higher robustness to resonance offsets, we link the reduced efficiency of DRF-SLIC to experimental imperfections.

Since, as detailed in Section 3, both PulsePol and DRF-SLIC allow scaling of the effective heteronuclear coupling in the SABRE complex, the observed higher performance (compared to SHEATH and SLIC) could be associated with two important factors. First, the reduced polarisation rate can be more suited for slow chemical exchange rather than a rapid one. Second, weaker effective heteronuclear coupling ensures high equivalence regime for the two hydride $^{1}$H spins, which in turn leads to more isolated polarisation build-up (see Fig. 4).

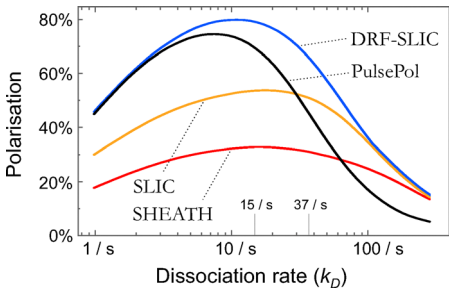


Fig. 5 Numerically optimised SABRE performance for hyperpolarisation of $^{15}$N-acetonitrile as a function of exchange rate using different polarisation transfer methods: SHEATH (red line), SLIC (orange line), PulsePol (black line) and DRF-SLIC (blue line). Simulation assumes a rapid parahydrogen exchange compared to the dissociation of a single $^{15}$N-molecule. Polarisation is evaluated after 20 s of its build-up.

However, reducing the effective coupling is not a good strategy in systems with exceedingly high dissociation rates. This is displayed by the less pronounced enhancement in polarisation for $^{15}$N-pyridine and the worse performance (relative to SHEATH and SLIC) observed for metronidazole.

Our simulation suggests that at high exchange rates, optimal conditions for DRF-SLIC converge back towards conventional SLIC where effective heteronuclear $J$-coupling is maximized and not reduced. At dissociation rates above 100 $\mathrm{s}^{-1}$, DRF-SLIC should not yield better results for SABRE systems with similar spin topology. The PulsePol method exhibits a tighter performance limit at exchange rates of around 40 $\mathrm{s}^{-1}$ and above. The likely reason is that PulsePol sequence relies on the pulse cycle completion for polarisation transfer. Thus, if the SABRE complex lifetime becomes comparable or shorter than the single PulsePol cycle, the polarisation cannot be successfully transferred from

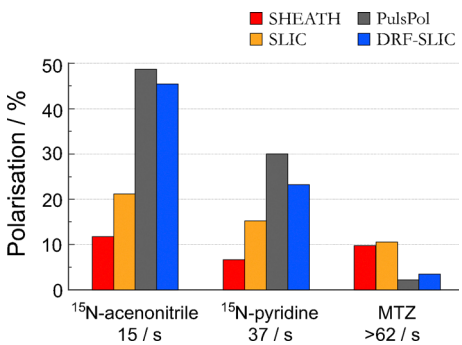


Fig. 6 $^{15}$N polarisation levels experimentally achieved using different optimised SABRE protocols shown in Fig. 3 for three different compounds: $^{15}$N-acetonitrile, $^{15}$N-pyridine, and metronidazole (MTZ). Experimentally determined dissociation rates at room temperature are given below. The metronidazole dissociation rate was estimated at 10 °C and thus is expected to be larger at room temperature.

the hydride to the $^{15}$N site causing a steep loss in performance. The polarisation yield using PulsePol may be recovered by lowering the sample temperature, as shown in the SI. Therefore, we expect that the overall best SABRE performance can be achieved by adjusting both the effective heteronuclear coupling with a suitable sequence and the chemical exchange dynamics with a chemical and physical modification of the system.

## Conclusions

In this study, we investigated three SABRE systems possessing similar spin–spin coupling topologies but distinct chemical exchange kinetics. These systems and the achieved $^{15}$N polarisation were compared by utilising four different SABRE polarisation transfer protocols. The highest performance was achieved using the PulsePol and DRF-SLIC protocols with $^{15}$N-acetonitrile approaching 50% of $^{15}$N polarisation. Compared to SABRE-SHEATH and SABRE-SLIC, these methods offer the adjustment of the effective heteronuclear coupling. We hypothesise that such reduction of the driving interaction can increase the overall SABRE performance due to improved matching with chemical exchange and more isolated spin dynamics. Evidently, this strategy is not optimal in systems displaying fast chemical exchange and may not be beneficial for systems exhibiting high magnetic equivalence (*e.g.* SABRE of $^{13}$C-pyruvate). However, a considerable variety of $^{15}$N-labelled SABRE substrates lie within these extremes and can lead to better results using sequences like PulsePol or DRF-SLIC. These methods should further complement cases where chemical dynamics are slowed down by the reduction of temperature or addition of co-ligands. Therefore, NMR protocols capable of adjusting effective spin coupling may lead to higher utility of SABRE applications.

## Conflicts of interest

The authors declare the following competing financial interests: V. P. K., B. A. R., I. S., S. K. and L. D. are or were employed by NVision Imaging Technologies GmbH. All other authors declare that they have no competing interests.

## Data availability

The experimental data and simulation scripts used in this manuscript are available at https://doi.org/10.5281/zenodo.18927246.

All data needed to evaluate the conclusions in the paper are present in the paper and the supplementary information (SI). Additional details on the experimental setup, optimisation routes as well as theoretical simulations are available in the SI. See DOI: https://doi.org/10.1039/d6cp00879h.

## Acknowledgements

L. D. would like to acknowledge the Marius Jakulis Jason foundation for their support and funding received by the Research Council of Lithuania (grant number S-MIP-25-24).

## References

1 C. R. Bowers and D. P. Weitekamp, *Phys. Rev. Lett.*, 1986, **57**, 2645–2648.
2 J. Eills, D. Budker, S. Cavagnero, E. Y. Chekmenev, S. J. Elliott, S. Jannin, A. Lesage, J. Matysik, T. Meersmann, T. Prisner, J. A. Reimer, H. Yang and I. V. Koptyug, *Chem. Rev.*, 2023, **123**, 1417–1551.
3 S. B. Duckett and R. E. Mewis, *Acc. Chem. Res.*, 2012, **45**, 1247–1257.
4 E. J. Fear, A. J. Kennerley, P. J. Rayner, P. Norcott, S. S. Roy and S. B. Duckett, *Magn. Reson. Med.*, 2022, **88**, 11–27.
5 P. Pham and C. Hilty, *Chem. Sci.*, 2023, **14**, 10258–10263.
6 T. Tennant, M. C. Hulme, T. B. Robertson, O. B. Sutcliffe and R. E. Mewis, *Magn. Reson. Chem.*, 2020, **58**, 1151–1159.
7 M. E. Gemeinhardt, M. N. Limbach, T. R. Gebhardt, C. W. Eriksson, S. L. Eriksson, J. R. Lindale, E. A. Goodson, W. S. Warren, E. Y. Chekmenev and B. M. Goodson, *Angew. Chem., Int. Ed.*, 2020, **59**, 418–423.
8 P. TomHon, M. Abdulmojeed, I. Adelabu, S. Nantogma, M. S. H. Kabir, S. Lehmkuhl, E. Y. Chekmenev and T. Theis, *J. Am. Chem. Soc.*, 2022, **144**, 282–287.
9 H. de Maissin, P. R. Groß, O. Mohiuddin, M. Weigt, L. Nagel, M. Herzog, Z. Wang, R. Willing, W. Reichardt, M. Pichotka, L. Heß, T. Reinheckel, H. J. Jessen, R. Zeiser, M. Bock, D. von Elverfeldt, M. Zaitsev, S. Korchak, S. Glöggler, J.-B. Hövener, E. Y. Chekmenev, F. Schilling, S. Knecht and A. B. Schmidt, *Angew. Chem., Int. Ed.*, 2023, **62**, e202306654.
10 A. N. Pravdivtsev, K. Buckenmaier, N. Kempf, G. Stevanato, K. Scheffler, J. Engelmann, M. Plaumann, R. Koerber, J.-B. Hövener and T. Theis, *J. Phys. Chem. C*, 2023, **127**, 6744–6753.
11 A. B. Schmidt, J. Eills, L. Dagys, M. Gierse, M. Keim, S. Lucas, M. Bock, I. Schwartz, M. Zaitsev, E. Y. Chekmenev and S. Knecht, *J. Phys. Chem. Lett.*, 2023, **14**, 5305–5309.
12 J. Z. Myers, M. Plaumann, K. Buckenmaier, A. N. Pravdivtsev and R. Körber, *Commun. Chem.*, 2025, **9**, 1–9.
13 S. L. Eriksson, J. R. Lindale, X. Li and W. S. Warren, *Sci. Adv.*, 2022, **8**, eabl3708.
14 X. Li, J. R. Lindale, S. L. Eriksson and W. S. Warren, *Phys. Chem. Chem. Phys.*, 2022, **24**, 16462–16470.
15 J. R. Lindale, L. L. Smith, M. W. Mammen, S. L. Eriksson, L. M. Everhart and W. S. Warren, *Proc. Natl. Acad. Sci. U. S. A.*, 2024, **121**, e2400066121.
16 D. A. Markelov, V. P. Kozinenko, A. V. Yurkovskaya and K. L. Ivanov, *J. Magn. Reson. Open*, 2023, **16–17**, 100139.
17 D. A. Markelov, V. P. Kozinenko, A. S. Kiryutin and A. V. Yurkovskaya, *J. Chem. Phys.*, 2024, **161**, 214203.

 This journal is © the Owner Societies 2026

18 V. P. Kozinenko, A. S. Kiryutin and A. V. Yurkovskaya, *Chem.: Methods*, 2025, **5**, e202400060.
19 T. Theis, M. Truong, A. M. Coffey, E. Y. Chekmenev and W. S. Warren, *J. Magn. Reson.*, 2014, **248**, 23–26.
20 M. L. Truong, T. Theis, A. M. Coffey, R. V. Shchepin, K. W. Waddell, F. Shi, B. M. Goodson, W. S. Warren and E. Y. Chekmenev, *J. Phys. Chem. C*, 2015, **119**, 8786–8797.
21 T. Theis, M. L. Truong, A. M. Coffey, R. V. Shchepin, K. W. Waddell, F. Shi, B. M. Goodson, W. S. Warren and E. Y. Chekmenev, *J. Am. Chem. Soc.*, 2015, **137**, 1404–1407.
22 M. Fekete, F. Ahwal and S. B. Duckett, *J. Phys. Chem. B*, 2020, **124**, 4573–4580.
23 S. Knecht, A. S. Kiryutin, A. V. Yurkovskaya and K. L. Ivanov, *Mol. Phys.*, 2019, **117**, 2762–2771.
24 I. Schwartz, J. Scheuer, B. Tratzmiller, S. Müller, Q. Chen, I. Dhand, Z.-Y. Wang, C. Müller, B. Naydenov, F. Jelezko and M. B. Plenio, *Sci. Adv.*, 2018, **4**, eaat8978.
25 B. Tratzmiller, J. F. Haase, Z. Wang and M. B. Plenio, *Phys. Rev. A*, 2021, **103**, 012607.
26 D. A. Barskiy, K. V. Kovtunov, I. V. Koptyug, P. He, K. A. Groome, Q. A. Best, F. Shi, B. M. Goodson, R. V. Shchepin, A. M. Coffey, K. W. Waddell and E. Y. Chekmenev, *J. Am. Chem. Soc.*, 2014, **136**, 3322–3325.
27 C. Bengs, L. Dagys and M. H. Levitt, *J. Magn. Reson.*, 2020, **321**, 106850.
28 A. N. Pravdivtsev, A. V. Yurkovskaya, N. N. Lukzen, K. L. Ivanov and H.-M. Vieth, *J. Phys. Chem. Lett.*, 2014, **5**, 3421–3426.
29 V. P. Kozinenko, A. S. Kiryutin, A. V. Yurkovskaya and K. L. Ivanov, *J. Magn. Reson.*, 2019, **309**, 106594.
30 A. N. Pravdivtsev, A. V. Yurkovskaya, H. Zimmermann, H.-M. Vieth and K. L. Ivanov, *RSC Adv.*, 2015, **5**, 63615–63623.
31 M. Sabba, N. Wili, C. Bengs, J. W. Whipham, L. J. Brown and M. H. Levitt, *J. Chem. Phys.*, 2022, **157**, 134302.
32 M. C. Korzeczek, L. Dagys, C. Müller, B. Tratzmiller, A. Salhov, T. Eichhorn, J. Scheuer, S. Knecht, M. B. Plenio and I. Schwartz, *J. Magn. Reson.*, 2024, **362**, 107671.
33 S. J. DeVience, R. L. Walsworth and M. S. Rosen, *Phys. Rev. Lett.*, 2013, **111**, 173002.
34 J. W. Pavlik and S. Laohhasurayotin, *J. Heterocycl. Chem.*, 2007, **44**, 1485–1492.
35 L. D. Vazquez-Serrano, B. T. Owens and J. M. Buriak, *Inorg. Chim. Acta*, 2006, **359**, 2786–2797.
36 R. E. Mewis, R. A. Green, M. C. R. Cockett, M. J. Cowley, S. B. Duckett, G. G. R. Green, R. O. John, P. J. Rayner and D. C. Williamson, *J. Phys. Chem. B*, 2015, **119**, 1416–1424.
37 A. S. Kiryutin, A. V. Yurkovskaya, H. Zimmermann, H.-M. Vieth and K. L. Ivanov, *Magn. Reson. Chem.*, 2018, **56**, 651–662.
38 D. A. Barskiy, A. N. Pravdivtsev, K. L. Ivanov, K. V. Kovtunov and I. V. Koptyug, *Phys. Chem. Chem. Phys.*, 2015, **18**, 89–93.
39 B. A. Rodin and K. L. Ivanov, *Magn. Reson.*, 2020, **1**, 347–365.
40 G. Stevanato, S. S. Roy, J. Hill-Cousins, I. Kuprov, L. J. Brown, R. C. D. Brown, G. Pileio and M. H. Levitt, *Phys. Chem. Chem. Phys.*, 2015, **17**, 5913–5922.

This journal is © the Owner Societies 2026